THE JOURNAL OF PHYSICAL CHEMISTRY A

ARTICLE

pubs.acs.org/JPCA

Structural Photodynamics of Camptothecin, an Anticancer Drug in Aqueous Solutions

Maria Rosaria di Nunzio, Boiko Cohen, and Abderrazzak Douhal*

Departamento de Química Física, Facultad de Ciencias Ambientales y Bioquímica, and INAMOL, Universidad de Castilla-La Mancha, Avenida Carlos III, S/N, 45071 Toledo, Spain

Supporting Information

ABSTRACT: Steady-state and time-resolved picosecond emission studies were carried out to study the role of the proton concentration in the acid−base properties of the anticancer drug camptothecin (CPT) in its ground and electronically first excited states. The results show that, under acidic conditions, the excited-state proton-transfer (ESPT) reaction is irreversible, in contrast to previous literature data. We found that the prototropic species are equilibrated at the excited state ($pK_a^* = 1.85$) only in a restricted range of pH ($1.5 < pH < 3$), whereas only one species, either the neutral form ($\tau_N = 3.76$ ns) or the protonated form ($\tau_C = 2.83$ ns), can be detected at pH > 3 and pH < 1.5, respectively. The proton motion from the acidic solution to the neutral form in the pH 1−2 domain is diffusion-controlled. Within the range of pH 1−2, the reaction rate constant for the formation (k_d) of the encounter complex between the proton and the neutral form ranges from 1.17×10^{10} to 7.33×10^{10} M^{-1} s^{-1}, respectively. Under more acidic conditions (pH 0.9−0.95), the protonation of CPT does not depend on the diffusive step, because of the large amount of protons. The direct proton-transfer rate constant (k_{DPT}^*) increases with the proton concentration (time constants change from 24 ps to ∼1 ns at pH 0.9 and 2, respectively). The number of protons involved in the proton transfer changes from approximately one, for the diffusive regime, to approximately four, for the static regime. We found good agreement between the Birks model for equilibrated flourophores and the Debye−Smoluchowski equation (DSE) to accurately explain the ESPT reaction of CPT with acidic water in the reversible range. The proton motion at pH 2 (equilibrium range) exhibits diffusion-controlled behavior and can be explained using the Smoluchowski model. Our results show that the interaction of CPT with acidic water depends on the concentration of the acid, which changes the nature of both the structure and dynamics.

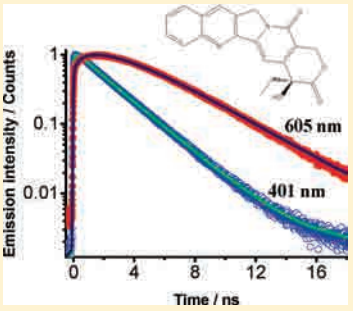

1. INTRODUCTION

The discovery of 20-(*S*)-camptothecin (CPT) dates from 1966, when Wall and Wani isolated it from the wood, bark, and fruit of the tree *Camptotheca acuminate* and established its whole structure.[1] This fluorescent compound was found to be a potent inhibitor of the growth of leukemia cells and of a wide range of experimental tumors[2] exerting an antidisease effect by inhibition of the nuclear enzyme topoisomerase I (topo I), which is essential for cell replication.[3−5] CPT expresses its cytotoxicity by binding reversibly to transient topo I−DNA covalent complexes, whose persistence significantly depends on the nature and strength of the binding (H-bonding and stacking interactions) between CPT and the flanking base pairs.[5a] Indeed, several studies of many promising anticancer, antiviral, and anti-inflammatory drugs have shown that their activity depends on the pH of the medium or/and light exposure.[6]

The CPT molecule, of interest here, consists of five rings, of which four (A, B, D and E) are six-membered and one (C) is five-membered (Scheme 1).

The A/B parts of CPT constitute the quinoline ring system, whereas a considerable electron-withdrawing effect is exerted by the pyridone D-ring. CPT is weakly soluble in water and not stable at physiological pH, where it converts rapidly by hydrolysis of the CPT-lactone to the corresponding ring-opened water-soluble carboxylate form (Scheme 1).[7] The CPT-lactone structure has a greater potency toward nonproliferation of tumor cells than the carboxylate form, which is generally inactive and more toxic than the lactone form. The lactone−carboxylate equilibrium is reversible and pH-dependent, with the lactone structure dominating at lower pH values ($pH \leq 6$). In human plasma, the carboxylate form becomes the principal species, and it shows a strong affinity to the serum albumin protein.[7]

Since its first isolation, studies of camptothecin and its analogues have been performed by many research groups, with the aim of finding more soluble, hydrolytically more stable, and less toxic CPT derivatives than the parent compound CPT.[8]

In the past two decades, the electronic and vibronic structures of CPT chromophores have been investigated by UV−visible absorption, fluorescence, and Raman spectroscopies.[9−13] The acid−base properties of the quinoline functional group of CPT were determined for both the ground state (S_0) and the first electronically excited state (S_1). Two different values of pK_a for CPT deprotonation at the quinoline $-NH^+$ site have been reported in the literature: about 0.7[10a] and 1.18.[9] In addition, the

Received: February 22, 2011
Revised: April 12, 2011
Published: May 02, 2011

Scheme 1. Molecular Structures of Equilibrated CPT-Lactone and CPT-Carboxylate Forms

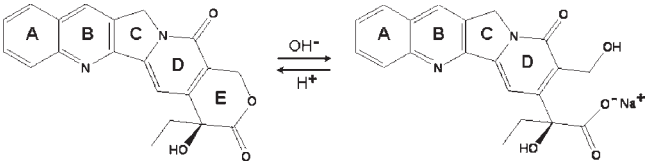

pK_a is very low when compared to that of quinoline (4.87).[14] This suggests that CPT is a weaker base than the quinoline ring at the S_0 state. Upon excitation to S_1, the pK_a^* value is 1.64.[10a] However, the effect is not as pronounced as in the case of other quinoline derivatives,[15] which display a stronger photobasicity ($\Delta pK_a = pK_a - pK_a^* \approx 10$).[15b]

The influence of pH on the acid−base properties of excited CPT has been mainly investigated by the use of stationary methods,[10] whereas there have been no reports on its photodynamics at different proton concentrations. The fluorescence lifetimes of the neutral (pH ≈ 5) and N-protonated (4 M $HClO_4$) forms are very similar (τ_F = 3.99 and 3.86, respectively).[10a] This suggests that an excited-state equilibrium is established during the lifetime of the excited species.

Herein, we report on steady-state (UV−visible absorption and emission) and time-resolved picosecond emission studies of CPT in aqueous solutions of different pH values (0.9−6) to obtain a better understanding of the role of the H-bonding surroundings in the structures and dynamics of protonation and deprotonation of the excited molecules. The obtained results show that, depending on the pH, it is possible to distinguish three ranges in which the drug behaves differently. In the more acidic range (pH 0.9−2) as well as in the pH 2−6 domain, the excited-state equilibrium between the cationic (C) and neutral (N) forms is not established. The former structure prevails at acid pH values, whereas the latter is the unique species detected at pH > 2. Excited C and N were found to be equilibrated only in the intermediate pH range (1.5 < pH < 3). Within this interval, the rate of proton motion is diffusion-controlled and increases with decreasing pH value. The number of hydronium ions ($n \approx 1$) directly connected to the excited CPT significantly increases to ∼4 at higher proton concentrations (pH ≤ 1). This result reflects the existence of two different reactions and proton motion dynamics. In the reversible range, we applied both the Birks model for equilibrated fluorophores and the Debye−Smoluchowski equation (DSE) for the proton motion, and we found good agreement between both models and the experimental behavior.

2. EXPERIMENTAL SECTION

(*S*)-(+)-Camptothecin (CPT) (Sigma-Aldrich, ∼95%), dimethylsulfoxide (DMSO) (Sigma-Aldrich, ≥99%), and anhydrous tetrahydrofuran (THF) (Sigma-Aldrich, ≥99.9%) were used as received. Deionized water, hydrochloric acid containing 33% HCl (Scharlau), potassium chloride (Panreac, >99%), and potassium dihydrogen phosphate (Merck, >99%) were used to prepare aqueous solutions of different pH values. The relative error of the measured pH was estimated to be around 2%. Steady-state absorption and emission spectra were recorded on Varian (Cary E1) and Perkin-Elmer LS 50B spectrophotometers, respectively. Emission lifetimes were measured by using a time-correlated single-photon-counting (TCSPC) spectrophotometer (FluoTime 200, PicoQuant). The sample was excited by a 40-ps pulsed (20 MHz) laser centered at 371 or 433 nm. The instrumental response function (IRF) of the apparatus was typically 65 ps. The fluorescence signal, gated at magic angle (54.7°), was monitored at a 90° angle to the excitation beam at discrete emission wavelengths using a 100-mm monochromator between the sample and the Hamamatsu microchannel plate photomultiplier (R3809-U21). The data were collected using a SPC 330 card. Decay data were analyzed using the FluoFit software package (PicoQuant). Exponential decay functions were convoluted with the experimental response function and fit to the experimental decay. The quality of the fits was characterized in terms of the reduced χ^2 value and the distribution of residuals. All measurements were done at 293 K.

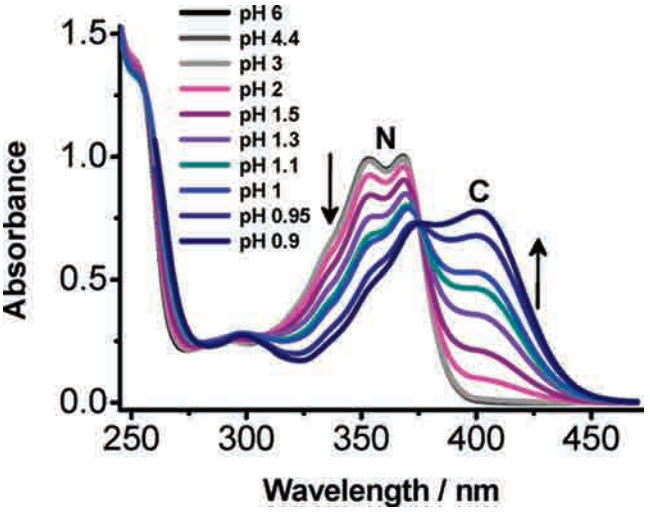

Figure 1. UV−visible absorption spectra of CPT in aqueous solutions as a function of pH. The $S_0 \rightarrow S_1$ absorption bands of neutral and cationic species are marked as N and C, respectively.

3. RESULTS AND DISCUSSION

3.1. Steady-State Observations. To gain a better understanding of the spectral properties of CPT, we first studied its steady-state behavior in THF, a noninteracting solvent, where the molecule is present in only its neutral form. The absorption spectrum of CPT in the range of 200−420 nm consists of four bands of $\pi-\pi^*$ nature, whose intensity and spectral position depend on the polarity, as well as the hydrogen-bonding ability of the solvent.[13] In THF (see the Supporting Information, Figure 1S), the long-wavelength $\pi-\pi^*$ band has intensity maxima at 385 (shoulder) and 368 nm. A vibronic interaction of the $^1\pi,\pi^*$ state with the close-lying $^1n,\pi^*$ state of the quinoline ring was suggested.[10b,13] Nevertheless, the $n-\pi^*$ transition is hidden by the two intense long-wavelength $\pi-\pi^*$ bands.

Although CPT is weakly soluble in water, aggregation can still occur even at low concentrations. Thus, to ensure complete solubilization of the drug and to avoid aggregation effects on our data, all solutions were prepared using 1/28 (v/v) DMSO/water mixtures (>0.99 molar fraction of H_2O). The concentration of the drug was $\sim 5 \times 10^{-5}$ M in all experiments. Figure 1 shows the UV−visible absorption spectra of CPT in aqueous solution at different pH values.

dx.doi.org/10.1021/jp201749u |*J. Phys. Chem. A* 2011, 115, 5094–5104

At pH 6, CPT predominantly exists in its neutral form. The intensity maxima of the $S_0 \rightarrow S_1$ band are at 353.5 and 368 nm. These transitions are UV-shifted by ~17 nm relative to those formed in THF, suggesting a lower dipole moment of excited CPT with respect to that in the ground state. Upon increasing the polarity of the environment, the CPT ground state is stabilized to a greater extent than the electronically excited one, and the absorption spectrum tends to move to higher energies. The H-bonding interactions with water through the unshared valence electron pairs of the D-ring carbonyl group of CPT also might contribute to the blue shift of its long-wavelength absorption maxima. This explanation is supported by theoretical calculations, which revealed that, upon excitation, the electron density is redistributed from the carbonyl group to the quinoline moiety, with the former becoming a charge donor at the S_1 state.[13] Interaction with a proton-donating solvent (such as water) prevents the charge-transfer process, thus destabilizing the excited state relative to the ground state. In addition, specific interactions with water molecules decrease the vibronic structure in the absorption spectrum. Upon acidification of the solution to pH 0.9, the spectrum gradually decreases in intensity, and concomitantly the quinolinium-type (C structrure) band appears in the long-wavelength range with a maximum at 401 nm. Two isosbestic points, at 375 and 255 nm, are clearly observed in the spectra. The molar extinction coefficients of N (ε_{368} = 27530 mol^{-1} L cm^{-1}) and C (ε_{401} = 22240 mol^{-1} L cm^{-1}) were obtained at near-neutral and acidic conditions, respectively (Supporting Information, Figure 2S). The ground-state pK_a value (deprotonation of the quinoline $-NH^+$ site) was obtained using the Henderson−Hasselbalch plot, as well as absorbance titration curves (Supporting Information, Figure 3S-A). We determined a value of pK_a = 1.14, which is very close to the reported value (pK_a = 1.18).[9] The main reason for the lower ground-state basicity of the quinoline nitrogen in CPT and its derivatives, compared to the unmodified quinoline, has been explained previously by the electron-withdrawing effect of the conjugated pyridone ring.[9,10a] The latter could also be protonated at high proton concentrations (the ground-state protonation of the 2-pyridone ring was found to occur under very acidic conditions, with a pK_a value of 0.32).[16] Semiempirical (AM1) calculations carried out for 10-hydroxy-substituted CPT (10-CPT) revealed that the hydroxypyridinium ion is stabilized with respect to the N-protonated quinolinium cation by ~4.4 kcal/mol.[17] However, because of their different solvation energies, it was difficult to provide an explicit information about the structure of the two tautomers. In summary, there are three contributing species to the absorption spectrum of CPT in aqueous solution: the neutral form, dominating at near-neutral pH values; the quinolinium-type structure, detectable under additional acidification of the solution; and the hydroxypyridinium ion, which might make a modest contribution under very acidic conditions.

The fluorescence of CPT is associated with the extended conjugation of the quinoline ring system.[13] The emission spectrum in THF (Supporting Information, Figure 1S) consists of a single wide band having a maximum intensity at 428 nm. The fluorescence quantum yield of CPT is moderately low in aprotic solvents (in cyclohexane, Φ_F = 0.47), whereas it increases in H-bonding ones (in water at pH 5.2, Φ_F = 0.64).[10b] This is mainly due to different solute−solvent interactions affecting the interplay between the $^1n,\pi^*$ and $^1\pi,\pi^*$ states.

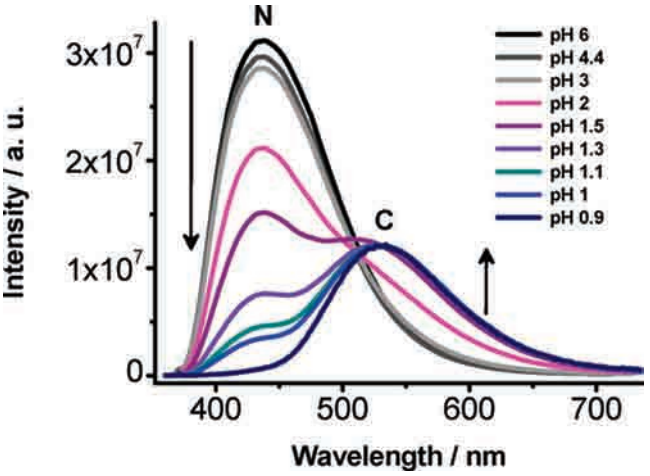

Figure 2. Corrected emission spectra of CPT in aqueous solution as a function of pH. The emission bands of neutral and cationic species are marked as N* and C*, respectively. The excitation wavelength is 371 nm, and the temperature is 293 K.

We recorded the emission spectra of CPT in aqueous solutions in the same range of pH as used for the absorbance measurements (Figure 2). The fluorescence intensities were corrected for the changes in absorbance.

For the solutions having pH 6−3, the emission principally comes from the excited neutral (N*) form (λ_{em} = 438 nm). A noticeable band broadening is observed in the spectra at pH < 2, and upon further decrease in the pH, a new band assigned to the excited cation (C*) appears, with a maximum of emission intensity at 530 nm. The decrease in pH also leads to a marked decrease in the N* band intensity. The lack of a clear isoemissive point suggests the existence of differently H-bonded C* structures.

The Stokes shifts ($\Delta\bar{\nu}_{ST}$) for N* and C* emissions are 4343 and 6070 cm^{-1}, respectively. The larger value of $\Delta\bar{\nu}_{ST}$ observed for C* indicates a larger vibrational relaxation of the excited protonated CPT with respect to its neutral form and, thus, a higher electronic redistribution after excitation.

To calculate the excited-state pK_a^* (1.85) we used the fluorescence titration curves, constructed from the relative fluorescence intensities at different wavelengths of observation (Supporting Information, Figure 3S-B). This value is in agreement with the previously reported one (pK_a^* = 1.65).[10a]

As mentioned above, in alkaline water solutions, the lactone ring of CPT hydrolyzes to produce CPT-carboxylate form.[7] The pK_a of the carboxylic group of CPT is about 6.5.[17] The rate of the ring-opening reaction is low at low pH values, but it increases with the pH. At pH > 5, the absorption and emission spectra show red shifts of ~5 and 20 nm, respectively.[10a] The fluorescence quantum yield of the CPT-carboxylate (Φ_F = 0.62 at pH 9.1) is similar to that of CPT (Φ_F = 0.64 at pH 5.1), whereas the lifetime of the CPT-carboxylate (τ_F = 4.48 at pH 9.1) is larger than that of CPT (τ_F = 3.99 at pH 5.1).[10a] The ratio of the relative fractions of CPT-lactone/CPT-carboxylate in the 5−8 pH range ranged from 0.99 (at pH 5.20) to 0.01 (at pH 8.0). At pH 5.94, 85% of the molecules are present in the ring-closed form, with an equilibrium constant of 0.16. Under our experimental conditions, a contribution (~10%) from the ring-opened form to the overall emission process was observed at pH > 3.

3.2. Picosecond Time-Resolved Emission Measurements. The fluorescence lifetime of the neutral form of CPT in THF, a

Table 1. Values of Fluorescence Time Constants (τ), Normalized Pre-Exponential Factors (A), and Normalized Contributions (C) for CPT in Water at High pH Values and at Different Emission Wavelengths (λ_{em})[a]

λ_{em} (nm)	τ (ns)	A (%)	C (%)
	pH 3		
410	3.45	100	100
440	3.47	100	100
490	3.63	100	100
530	4.06	100	100
	pH 4.4		
410	3.69	100	100
440	3.71	100	100
490	3.80	100	100
530	4.05	100	100
	pH 6		
410	3.71	100	100
440	3.74	100	100
490	3.81	100	100
530	4.03	100	100

[a] Excitation wavelength = 371 nm, and T = 293 K.

noninteracting solvent, was measured to be 2.98 ± 0.05 ns (Supporting Information, inset of Figure 1S), which agrees with the reported value (τ_F = 2.96 ± 0.02 ns).[10b] To obtain information on the mechanism of proton motion from the solvent to the excited CPT in the pH range from 0.9 to 6, we recorded the emission decays at different observation wavelengths. In this case, the excitation wavelengths were 371 and 433 nm. We observed different behaviors according to the experimental conditions, as described in the following sections.

pH > 2 For the related solutions, the only emitting species is N*. The fluorescence emission decays show a monoexponential behavior throughout the entire range of observation wavelengths, giving a lifetime of τ_N = 3.76 ns (Table 1), different from that observed in THF (~3 ns). The difference reflects the H-bonding and polarity effects on the coupling between the $^1n,\pi^*$ and $^1\pi,\pi^*$ states.

pH < 2 Under very acidic conditions, the emission decays were fit to a biexponential function, independently of the observation wavelength. Figure 3 shows four typical emission decays of CPT in water at pH 1. It is clear that the dynamics of the excited CPT relaxation changes with the observation wavelength, where N* (410, 440 nm) or C* (490, 530, and 605 nm) can emit.

Table 2 gives the values obtained for the time constants (τ_i), normalized pre-exponential factors (A_i), and normalized contributions (C_i) in the emission decays of CPT in the studied solutions.

Short (τ_1 = 0.2−2 ns) and long ($\tau_2 \approx$ 2.9 ns) components were determined with a good accuracy from a global analysis ($\chi^2 \leq 1.1$). The short component (τ_1) rises at 530 and 605 nm and corresponds to a decay at higher energies (410−490 nm). The latter largely contributes to the signals at 410 and 440 nm: A_1 > 98% at the investigated pH values. We observed a significant increase in the τ_1 value (from 203 ps at pH 0.9 to 1.29 ns at pH 1.5) when the proton concentration was gradually decreased from 0.12 to 0.03 M (Table 2 and Figure 4).

The slow component (τ_2) prevails throughout the red side (490−605 nm) of the spectrum. Its contribution reaches a maximum at 530 nm (A_2, 86%; C_2, 99% at pH 0.9), whereas on the bluest side, this component becomes very weak. However, with increasing pH, its contribution in the red decreases slightly. Thus, we assign the fast and slow components to emissions from N* and C*, respectively.

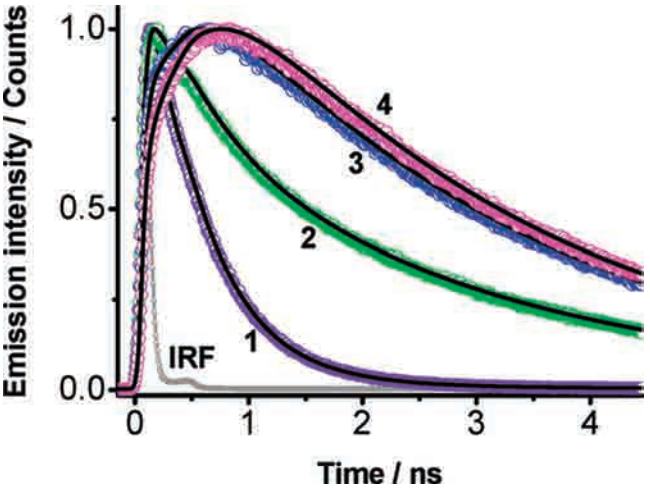

Figure 3. Emission decays of CPT in water (pH 1) gated at (1) 440, (2) 490, (3) 530, and (4) 605 nm. The solid lines are the best-fit exponential functions, and IRF is the instrumental response function (IRF, 60 ps). Excitation was at 371 nm, and T was 293 K.

The establishment of an equilibrium in the S_1 state between the two structures leads to similar decay time constants. However, in our experiments, we observed that τ_1 and τ_2 have different values, especially at low pH values. Moreover, in acidic solutions (0.9 ≤ pH ≤ 1.3) and with excitation at 433 nm (Table 3), where only the cationic form absorbs (Figure 1), the fluorescence decays showed a clear monoexponential behavior giving a lifetime of 2.83 ns, similar to the τ_2 value.

Thus, the results suggest that, at pH < 2, the N* and C* forms are not in equilibrium at S_1. Further support for this conclusion is given by the absence of emission from N* in acidic solutions (0.9 ≤ pH < 2) and upon excitation at 433 nm (Supporting Information, Figure 4S).

In the 1 ≤ pH ≤ 2 range, we observed a quenching of N* emission by protons in the steady-state spectra. The data were analyzed using a Stern−Volmer equation to second order in $[H^+]$ (eq 1 and Figure 5).

$$\frac{F_0}{F} = (1 + K_D[H^+])(1 + K_S[H^+]) \quad (1)$$

In eq 1, F_0 and F are the fluorescence intensities of N* in the absence (determined in the pH 3−6 range) and presence, respectively, of an excited-state proton-transfer reaction, and K_D and K_S are the dynamic and static quenching constants, respectively. The characteristic upward curvature of the Stern−Volmer plot (Figure 5) indicates a static quenching of N* emission, accompanying the overall dynamic quenching process. The dynamic portion of the observed quenching was determined by lifetime measurements using the equation

$$\frac{\tau_0}{\tau} = 1 + K_D[H^+] \quad (2)$$

where τ_0 is the lifetime of unquenched N* emission measured in the pH 3−6 range and τ is the time constant of the fast

dx.doi.org/10.1021/jp201749u |J. Phys. Chem. A 2011, 115, 5094–5104

Table 2. Values of Fluorescence Time Constants (τ_i), Normalized Pre-Exponential Factors (A_i), and Normalized Contributions (C_i) for CPT in Water at Low pH Values and at Different Emission Wavelengths (λ_{em})[a]

λ_{em} (nm)	τ_1 (ps)	A_1 (%)	C_1 (%)	τ_2 (ns)	A_2 (%)	C_2 (%)
			pH 0.9			
410	203	99	91	2.81	1	9
440	203	98	79	2.81	2	21
490	203	28	3	2.81	72	97
530	203	(−)14	(−)1	2.81	86	99
605	203	(−)21	(−)2	2.81	79	98
			pH 0.95			
410	261	99	91	2.81	1	9
440	261	98	82	2.81	2	18
490	261	32	4	2.81	68	96
530	261	(−)17	2	2.81	83	98
605	261	(−)25	(−)3	2.81	75	97
			pH 1			
410	549	99.7	98	2.81	0.3	2
440	549	99	93	2.81	1	7
490	549	37	9	2.81	63	91
530	549	(−)26	(−)6	2.81	74	94
605	549	(−)34	(−)8	2.81	66	92
			pH 1.1			
410	603	99.7	99	2.83	0.3	1
440	603	99	95	2.83	1	5
490	603	38	12	2.83	62	88
530	603	(−)28	(−)8	2.83	72	92
605	603	(−)36	(−)11	2.83	64	89
			pH 1.3			
410	858	99.7	99	2.84	0.3	1
440	858	99	96	2.84	1	4
490	858	39	16	2.84	61	84
530	858	(−)32	(−)12	2.84	68	88
605	858	(−)40	(−)17	2.84	60	83
			pH 1.5			
410	1.29	99	98	2.88	1	2
440	1.29	98	96	2.88	2	4
490	1.29	36	22	2.88	64	78
530	1.29	(−)37	(−)22	2.88	63	78
605	1.29	(−)44	(−)28	2.88	56	72
			pH 2			
410	2.25	87	84	2.98	13	16
440	2.25	86	82	2.98	14	18
490	2.25	11	9	2.98	89	91
530	2.25	(−)42	(−)35	2.98	58	65
605	2.25	(−)47	(−)40	2.98	53	60

[a] Excitation wavelength = 371 nm, and T = 293 K.

component of the quenched N* emission. The experimental data were satisfactorily fit, giving a squared correlation constant of $R^2 \approx 0.966$. The dynamic and static quenching constants were found to be K_D = 70.6 M^{-1} and K_S = 11.9 M^{-1}, respectively. The fluorescence quenching mechanisms of free CPT and

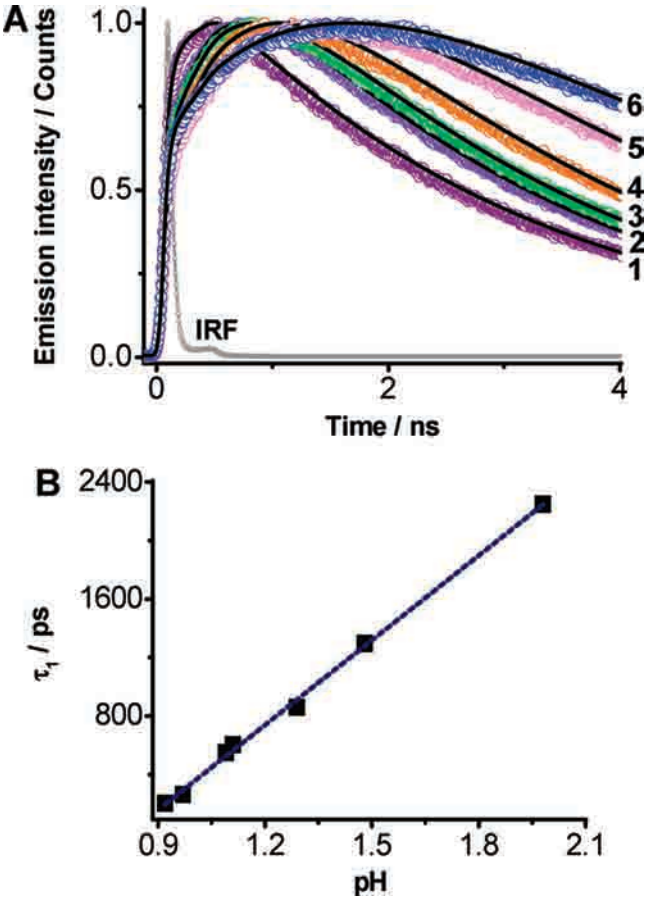

Figure 4. (A) Emission decays of CPT in water gated at 605 nm at pH (1) 0.9, (2) 1, (3) 1.1, (4) 1.3, (5) 1.5, and (6) 2. The solid lines are the best-fit exponential functions, and IRF is the instrumental response function. Excitation was at 371 nm, and T was 293 K. (B) Change of the fast time constant (τ_1) as a function of pH. The dashed line is just to guide the eyes.

Table 3. Values of Fluorescence Time Constants (τ), Normalized Pre-Exponential Factors (A), and Normalized Contributions (C) for CPT in Water at Low pH Values and at Two Emission Wavelengths (λ_{em})[a]

λ_{em} (nm)	τ (ns)	A (%)	C (%)
	pH 0.9		
490	2.84	100	100
590	2.84	100	100
	pH 1		
490	2.83	100	100
590	2.83	100	100
	pH 1.1		
490	2.83	100	100
590	2.84	100	100
	pH 1.3		
490	2.83	100	100
590	2.84	100	100

[a] Excitation wavelength = 433 nm, and T = 293 K.

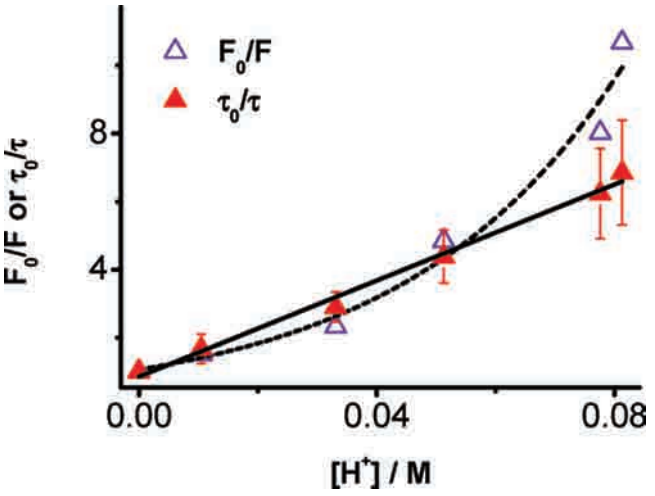

Figure 5. Fluorescence quenching of neutral CPT by the protons in aqueous solutions (open triangles, F_0/F; solid triangles, τ_0/τ). The nonlinear Stern−Volmer fit (dashed line) and a linear fit (straight line) are shown. The error bars for the lifetime plot are included.

CPT-carboxylate, as well as protein and liposome-bound CPT, have been previously investigated.[10b,18] Static and dynamic quenching of CPT in water at pH 5.1 in the presence of I^- ions (with the I^- concentration varying from 0 to 0.2 M) were observed and quantified (K_D = 33.7 M^{-1}, K_S = 4.0 M^{-1}, and τ_0 = 3.82 ns).[10b] Even though the mechanism of CPT fluorescence quenching by I^- ions is different from the mechanism reported here, a comparison can be made, because fluorescence quenching by collisions and by complex formation should not be very different in nature in the two systems. In the case of the CPT-carboxylate form (pH 9.2), the quenching was only dynamic in nature. It was also less efficient than that for the lactone form, with a constant value of K_D = 18.6 M^{-1} (τ_0 = 4.31 ns).[10b]

When the iodide concentration was increased (from 0 to 0.5 M), the observed K_D value for the fluorescence quenching of CPT by I^- ions was 44.3 M^{-1}.[18] Additionally, the iodide was found to form a static complex with the drug only when the molecule was free in solution.[18] In the presence of a lipid bilayer, the membrane-bound drug is less accessible to iodide and, thus, shows only dynamic quenching.[18]

Based on these observations, we describe the reaction of N* accepting a proton from the acidic water using a two-step diffusive model[19] (Scheme 2), where $N^*\cdots H_3O^+$ and $C^*\cdots H_2O$ are the H-bonded complexes of N* with the hydrated proton and of C* with the water molecule, respectively. The excited-state protonation of N*, which is irreversible under these conditions, is characterized by a rate constant, k^*_{DPT}, of a direct reaction. k_d is a bimolecular collisional rate constant typical for a system in a diffusion regime and is given by the Debye−Smoluchowski equation

$$k_d = \frac{4\pi N_A D R_D}{[1 - \exp(-R_D/a)]1000} \quad (3)$$

where N_A is Avogadro's number; D is the relative photobase-proton diffusion coefficient; R_D is the Debye radius; and a is the typical reaction contact radius, which, for H_3O^+, ranges from 5.5 to 8 Å.[17,20] We used a = 5.5 Å, the same as for the excited-state proton-transfer (ESPT) reaction of 10-hydroxycamptothecin (10-CPT) in water−methanol mixtures.[17] The Debye radius,

Scheme 2. Schematic Illustration of the Excited-State Protonation of Neutral CPT (N*) in the pH 1−2 Domain[a]

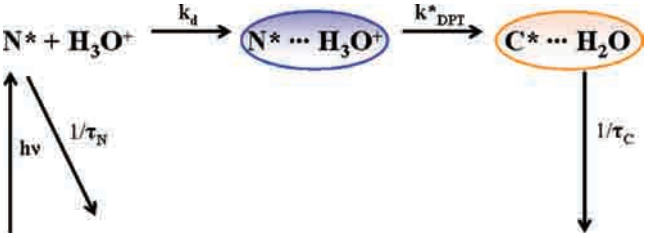

[a] $1/\tau_N$ and $1/\tau_C$ are the radiative rate constants for N* and C*, respectively; k_d is the rate constant for the diffusion process between the proton and N*; and k^*_{DPT} is the direct proton-transfer rate constant.

$R_D \equiv |z_1 z_2| e^2/k_B T\varepsilon$ (where $z_{1,2}$ and e are the ionic and electronic charges, respectively; ε is the dielectric constant of the medium; k_B is the Boltzmann constant; and T is the temperature), defines the Coloumbic attraction between the proton and the excited neutral form. The dielectric constant of each acidic solution was obtained from literature data.[21] The mutual diffusion coefficient, $D = D_{H^+} + D_{N^*}$, depends on the acid concentration. The proton diffusion coefficient was calculated using the Nernst equation[22] (see Supporting Information, eq 1S). The proton mobility was estimated from electrochemical data on equivalent conductance for HCl at several concentrations at 25 °C [concentration (equiv dm^{-3})][23] and number of transferred protons in water.[24] The diffusion constant, D_{N^*}, of the neutral form was evaluated from the Stokes−Einstein relationship

$$D = \frac{k_B T}{6\pi\eta R} \quad (4)$$

where η is the viscosity of the solution. In pure water, its value is 0.35×10^{-5} cm^2 s^{-1}. It was scaled to its value in HCl solutions (HCl-S) using the viscosity ratio $\eta_{H_2O}/\eta_{HCl\text{-}S}$ (the data on the viscosities of HCl solutions were estimated from ref 25). The diffusion-controlled reaction rate constant, k_s, for separation of the reaction complex was calculated using the equation

$$k_s = \frac{4\pi N_A D R_D}{[\exp(R_D/a) - 1]1000} \quad (5)$$

The relevant parameters for the diffusion step of N* and protons in the pH 1−1.5 range are summarized in Table 4.

The mutual diffusion constant, D, is influenced by the acid concentration (Table 4), decreasing when the latter increases (D = 1.54 and 3.28 $\times 10^{-5}$ cm^2 s^{-1} at pH 1 and 1.5, respectively). The observed decrease is due to the reduction in the proton mobility at higher hydrogen ion concentrations, which, in turn, affects the D_{H^+} values.[24a] At pH 1−1.3, a large number of collisions between the proton and N* have sufficient energy to make the complexes reactive, with the ratio $k_q/k_d \geq 1$. With an increase in the pH to 1.5, the energy barrier for the diffusive step between separated N* and H_3O^+ to form the encounter complex increases, as clearly evidenced by the reduction of the ratio k_q/k_d (k_q/k_d = 0.76 at pH 1.5).

The overall recombination steady-state rate constant (k_{on}) is given by[26]

$$k_{on} = \frac{k_q k^*_{DPT}}{k_s + k^*_{DPT}} \quad (6)$$

dx.doi.org/10.1021/jp201749u |J. Phys. Chem. A 2011, 115, 5094–5104

Table 4. Values of the Relevant Parameters for the Diffusion Step of N* and Proton Species in the pH 1−2 Range[a]

pH	$D_{H^+} \times 10^{-5}$ ($cm^2\ s^{-1}$)	$D_{N^*} \times 10^{-6}$ ($cm^2\ s^{-1}$)	$D \times 10^{-5}$ ($cm^2\ s^{-1}$)	R_D (Å)	$k_d \times 10^{10}$ ($M^{-1}\ s^{-1}$)	k_q/k_d	$k_s \times 10^{10}$ ($M^{-1}\ s^{-1}$)
1	1.19	3.51	1.54	7.43	1.17	1.61	0.079
1.1	1.25	3.51	1.60	7.42	1.21	1.55	0.082
1.3	1.89	3.51	2.24	7.37	1.69	1.11	0.12
1.5	2.93	3.52	3.28	7.34	2.47	0.76	0.17
2.0	9.41	3.52	9.76	7.29	7.33	0.26	0.52

[a] See text for clarity.

Scheme 3. Illustration of the Excited-State Protonation of Neutral CPT (N*) at High (pH < 1) Proton Concentrations[a]

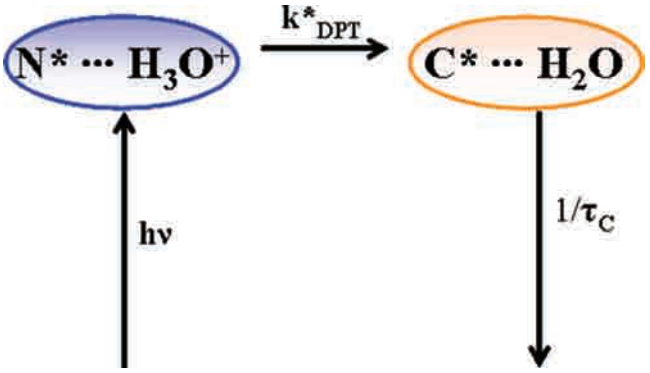

[a] $1/\tau_C$ is the radiative rate constant for C*, and k^*_{DPT} is the direct proton-transfer rate constant.

Scheme 4. Excited-State Protonation of Neutral CPT (N*) at pH 2[a]

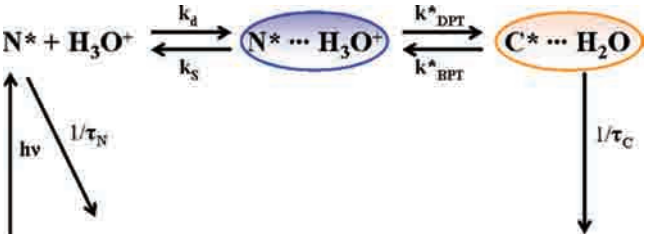

[a] $1/\tau_N$ and $1/\tau_C$ are the radiative rate constants for N* and C*, respectively; k_d and k_s are the rate constants for the diffusion and separation processes, respectively, between the proton and N*; and k^*_{DPT} and k^*_{BPT} are the direct and back proton-transfer rate constants, respectively.

For a reaction near the diffusion-controlled limit, the diffusion rate constant for the separation of the reaction complex (k_s) is lower than the rate constant for the direct proton-transfer reaction k^*_{DPT}, and thus eq 6 transforms into

$$k_{on} \approx k_q \quad (k^*_{DPT} > k_s) \tag{7}$$

Obviously, the ESPT reaction involves electronically excited species, and thus, one should consider the fluorescence lifetimes, namely, $1/k_N = \tau_N$, for the neutral form and $1/k_C = \tau_C$ for the protonated H-bonded form $C^*\cdots H_2O$. Emission from $N^*\cdots H_3O^+$ was not observed under our experimental conditions. Spectroscopic and dynamical data did not provide any evidence about the occurrence of radiationless proton-induced quenching of $N^*\cdots H_3O^+$ and $C^*\cdots H_2O$. Thus, we excluded a possible competition of the direct and back ESPT reactions with the proton-induced deactivation of $N^*\cdots H_3O^+$ and $C^*\cdots H_2O$ to the ground state. The kinetic equations that describe the irreversible behavior of the system are given in the Supporting Information. Under these experimental conditions, proton ejection from C* is much slower than both reprotonation of N* and deactivation of C*, so k^*_{BPT} (back reaction) can be neglected in the calculations.

At pH < 1, emission from N* cannot be detected (Figure 2). Thus, the average distance between the reactants could be less than 5.5 Å (typical reaction contact radius of H_3O^+). Therefore, the photoprotonation is triggered by the laser excitation in the reactants that are already complexed in the ground state (Scheme 3). The ESPT rate constant can be evaluated directly from the fast component τ_1, derived from the biexponential fit to the experimental data (Table 2). The lack of a rising component, expected at lower energies (530 and 605 nm), indicates a process faster than the time resolution of our detection system (~15 ps). Ultrafast (femtosecond regime) spectroscopic techniques can provide the time constant of the involved events. Such experiments are planned by this group for the near future.

pH ≈ 2. At this pH, equilibrium between N* and C* is established. As Table 2 shows, the smallest discrepancy of τ_1 (2.25 ns) from τ_2 (2.98 ns) is obtained, reducing $[H^+]$ by as much as 0.01 M. In addition, direct excitation of C (at 433 nm) leads to the appearance of emission from N* (Supporting Information, Figure 4S), whose formation is clear evidence of the existence of an excited-state equilibrium between the two structures. In this particular case, the rate constant of proton ejection from C* becomes comparable to that for reprotonation of N*, and it can compete with the deactivation of C* to the ground state (Scheme 4).

We calculated the mutual diffusion constant D at pH 2 to be $9.76 \times 10^{-5}\ cm^2\ s^{-1}$ ($D_{H^+} = 9.41 \times 10^{-5}\ cm^2\ s^{-1}$, $D_{N^*} = 3.52 \times 10^{-6}\ cm^2\ s^{-1}$, and $R_D = 7.29$ Å; see Table 4). The diffusion rate constant ($k_d = 7.33 \times 10^{10}\ M^{-1}\ s^{-1}$, Table 4) is almost 4 times larger than the quenching rate constant, $k_q = 1.88 \times 10^{10}\ M^{-1}\ s^{-1}$. The molecular dynamics is efficiently slowed with respect to that at low pH values, and the separation rate constant ($k_s = 0.52 \times 10^{10}\ M^{-1}\ s^{-1}$, Table 4) of the reaction complex becomes competitive with the proton-transfer rate constant.

To evaluate the direct and back ESPT rate constants, we applied the Birks model for equilibrated fluorophores[27] in the pH range of equilibrium between N* and C*. It is worth noting that the ratio of the pre-exponential factors of the decay and rise components, when the red emission is gated, is almost −1, indicating that C* is not reached by direct excitation, but rather comes from N* upon fast protonation by the hydrogen ion, once $N^*\cdots H_3O^+$ is formed by a diffusion-controlled

Table 5. Values of the Direct (k^*_{DPT}) and Back (k^*_{BPT}) Proton-Transfer Rate Constants and Other Related Parameters for CPT in HCl Solution

pH	$k^*_{DPT} \times 10^{10}$ (s^{-1})	τ_{DPT} (ps)	$k^*_{BPT} \times 10^{7}$ (s^{-1})	τ_{BPT} (ns)	K^*_{DPT}	$a_{H_3O^+}$ [a]
0.9	4.16	24	no equilibrium			0.1029
0.95	3.57	28				0.0918
1	0.654	153				0.0698
1.1	0.535	187				0.0667
1.3	0.495	202				0.0443
1.5	0.278	360				0.0288
2	0.106[b]	939[b]	8.33[b]	12[b]	12.78[b]	0.0095

[a] From ref 30. [b] Values obtained from the Birks model for equilibrated species.

process. Thus, the blue (I_B) and red (I_R) emission intensities can be written as

$$I_B = A_{1B}e^{-t/\tau_1} + A_{2B}e^{-t/\tau_2} \quad (8)$$

$$I_R = A_{1R}e^{-t/\tau_1} + A_{2R}e^{-t/\tau_2} \quad (9)$$

where τ_1 and τ_2 are the fast and the slow components, respectively, and A_{1B}, A_{2B} and A_{1R}, A_{2R} are the pre-exponential factors in the blue and red ranges, respectively. Equations 8 and 9 (more details are given in the Supporting Information) give the time constants of the direct and back proton-transfer reactions. A_{2R} and A_{1R} were found to be similar only at pH 2 ($A_{2R}/A_{1R} = -1.13$). In contrast, for larger proton concentrations, the ratio was always greater than -1, with a maximum value of -3.76 at pH 0.9. This result provides further confirmation of the irreversibility of the protonation for excited CPT at low pH values. Table 5 lists the values obtained for the rate (time) constants.

The present data show how the dynamics of excited CPT are strongly influenced by the proton concentration even when the acidity of the surrounding medium varies within a small range. At low pH values (pH 0.9−0.95), because of the formation of ground-state H-bonded complexes of N, the ESPT reaction is close to the "static" reaction limit (i.e., a reaction that does not involve a preliminary diffusion step). The obtained time constant for the direct proton transfer, τ_{DPT}, at pH 0.9 is 24 ps. It does not change significantly (28 ps) when the pH is increased to 0.95. At pH ≥ 1, diffusion governs the dynamics of protonation. In this case, the time constants for proton transfer are at least 5 times greater than those found in the limit range, where diffusion does not play a key role (τ_{DPT} = 153 and 360 ps at pH 1 and 1.5, respectively). The time constants for the direct and back proton-transfer reactions in the reversible range (pH 2) are increased, reaching almost 1 ns for the direct process (Table 5).

The ESPT reaction of CPT at acidic pH values can be considered as a tunnelling reaction through the activation energy barrier provided by the solvent.[28] The time scale of proton motion in this case is considerably longer than the time constants of other relevant motions (intramolecular vibrations or solvent translations or rotations). The model applied here is described by a two-level scheme (corresponding to the proton being in the reactant or product well) separated by an energy barrier in a double minimum in the potential energy surfaces. The activation energy for the tunnelling reaction was assumed to not correspond to the barrier

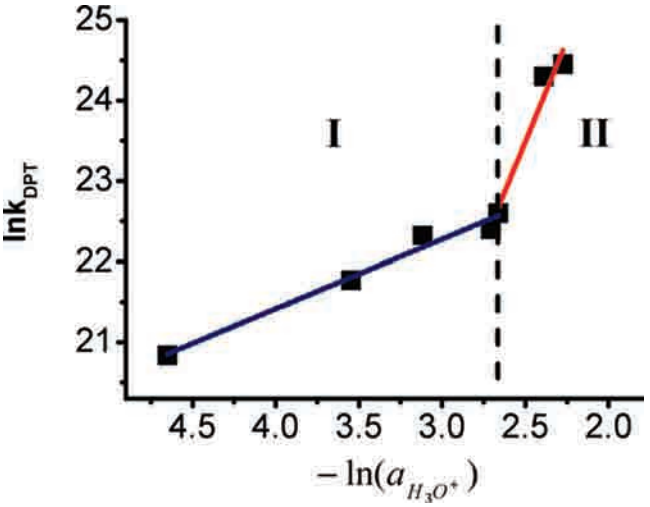

Figure 6. Linear fit of the logarithm of the direct proton-transfer rate constant (k_{DPT}) as a function of the logarithm of the hydrogen ion activity in the used aqueous solutions.

along the proton coordinate but rather to arise from the reorganization energy of the solvent required to approximately balance the energy of the proton in the two states. For CPT in water having high proton concentrations, the activation energy required for solvent reorganization should be very low. As a consequence, the ESPT process becomes energetically favorable, and the rate constant for protonation decreases considerably.

The correlation between k^*_{DPT} and the activity of H_3O^+ can be analyzed according to the empirical expression[17,29]

$$\ln k^*_{DPT} = \ln(k^*_{DPT})_0 + n \ln(a_{H_3O^+}) \quad (10)$$

where $a_{H_3O^+}$ is the activity of H_3O^+ and n reflects the number of protons involved in the retro-proton-transfer step.[30] $(k^*_{DPT})_0$ is the rate constant of protonation when $a_{H_3O^+} = 1$ and, thus, the intrinsic proton-transfer rate constant in the static reaction limit. Figure 6 shows the results obtained using the eq 10 to fit the experimental data.

Two ranges can be clearly distinguished (I and II): In the first one (I, pH 2−1), we obtained $n \approx 1$, $(k^*_{DPT})_0 = 6.27 \times 10^{10}$ s^{-1}, and $(\tau_{DPT})_0$ = 16 ps from the slope and intercept, respectively. For the more acidic range (II, pH 1−0.9), the data were best fit using a linear function with higher values for the slope and intercept: $n = 4 \pm 1$, $(k^*_{DPT})_0 = 5.10 \times 10^{12}$ s^{-1}, and $(\tau_{DPT})_0$ = 0.2 ps, respectively. It has been proposed that the proton transfer in bulk water is the result of a continuous fluctuation between $H_9O_4^+$ (Eigen cation), corresponding to one H_3O^+ species surrounded by three water molecules (first solvation shell), and $H_5O_2^+$ (Zündel cation), corresponding to a complex in which the proton is shared between two H_2O molecules.[24a] The determination of the microscopic nature of proton hydration is based on the efforts of numerous groups that have carried out several molecular dynamics simulations of H_3O^+ in H_2O over the past 20 years.[24b−d] Recently, the vibrational spectrum of protonated water clusters has been investigated, and it was suggested that the presence of signature bands indicates the existence of embedded Eigen or Zündel limiting forms.[24e] The influence of excess protons on the vibrational energy relaxation of the O−H and O−D stretching modes in water was studied using femtosecond pump−probe spectroscopy.[24f]

Scheme 5. Two-Step Scheme for the Application of the Debye−Smoluchowski Equation (DSE) to the ESPT Reaction of CPT with Acidic Water in the Reversible Range[a]

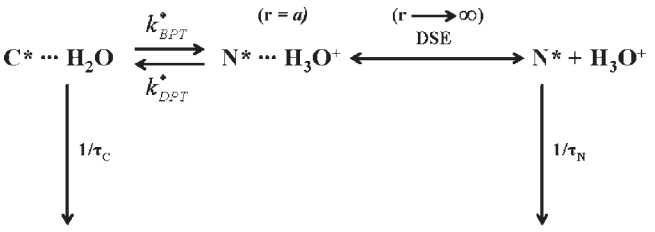

[a] $1/\tau_N$ and $1/\tau_C$ are the radiative rate constants for N* and C*, respectively; k^*_{DPT} and k^*_{BPT} are the direct and back proton-transfer rate constants, respectively; and r is the length (in angstroms) of the contact radius in the ion pair.

The meaning of fast proton jump in water to give either Eigen or Zündel hydrogen ions is the consequence of the low energetic barrier (2.6 kcal/mol) needed for the interconversion between the two structures.[24a] The two proton complexes occur with approximately the same probability. Therefore, we associate $n \approx 1$ with the number of hydrogen ions (either Eigen or Zündel) in contact with the CPT molecule in the first range of pH (2−1). These observations indicate that a H-bond network is necessary for the dissociated proton to move from one water molecule to another and, finally, to the nitrogen atom of the quinoline moiety, thus explaining the general slowing of the ESPT processes for CPT in the diffusion-controlled range.[31] The value of $(\tau^*_{DPT})_0$ is 16 ps, which represents the time constant for proton transfer from acidic water to the N* molecules, forming a H-bonded complex in the ground state. Changes in the solution structure (due to different proton concentrations and ionic strengths), which cause an energetic discrepancy between the different forms of protonated water ($H_5O_2^+$, $H_9O_4^+$, or H_3O^+), have an effect on the mobility of protons and, as a consequence, on the proton ejection rate constant from CPT to the surrounding medium. It has been observed that, in hydrochloric acid solutions, the structures of solvated H^+ and Cl^- ions are affected by the acid concentration.[24a] In particular, when the acid concentration increases, new H-bonds between Cl and H are formed, the H-bond between H_3O^+ and the closest water molecule is shorter, and the number of solvation shells of H_3O^+ decreases. These factors ultimately contribute to the decrease of the proton mobility. The higher value of n (4 ± 1) found in very acidic conditions (pH 1−0.9) reflects the probability of finding protons in the outer solvation shell. The H-bonding interaction of protons with the carbonyl groups of the D- and/or E-rings, which become stronger at high proton concentrations, might be responsible for the high value found for $(k^*_{DPT})_0$. The $(\tau^*_{DPT})_0$ value (200 fs) is close to that (170 fs) found for the formation of the H-bonds in water molecules.[32]

As shown before, the photophysics of CPT in apolar, aprotic sovents, such as THF, where CPT is present only in its neutral form, is characterized by monoexponential fluorescence decay. In water solution at pH > 2, only the emission from N* is observed, whereas detection of both the N* and C* forms becomes possible at higher proton concentrations (pH < 2). In this range, the ESPT reaction is irreversible (Scheme 2), because N* and C* are not equilibrated. Diffusion has a role in the protonation at pH 1−2, whereas, under extreme acidic conditions, the reaction occurs without the diffusive step. Equilibrium between the two forms is detected only at pH 2.

Table 6. Values of the Parameters Used in Fitting the Time-Resolved Fluorescence Decays of CPT and Calculated pK^*_a Values at pH 2 (Reversible Range)[a]

parameter	value	parameter	value
pH	2	τ_{DPT} (ps)	917
k^*_{BPT} (ns^{-1})	0.086	R_D (Å)	7.29
τ_{BPT} (ns)	11.63	$D \times 10^{-5}$ ($cm^2\ s^{-1}$)	9.80
k^*_{DPT} (Å ns^{-1})	6	pK^{*b}_a	1.78
$k_a{}^c$ ($Å^3\ ns^{-1}$)	2281		

[a] Fitting based on numerical resolution of the Debye−Smoluchowski equation (DSE), for which more detailed descriptions of the theory and method are given in refs 33−35. [b] Excited-state pK^*_a was calculated as $pK^*_a = -\log\{[k^*_{BPT}10^{27}\exp(-R_D/a)]/(k_aN_A)\}$. The value of the contact radius in the ion pair, a, was assumed to be 5.5 Å. [c] $k_a = 4\pi a^2 k^*_{DPT}$.

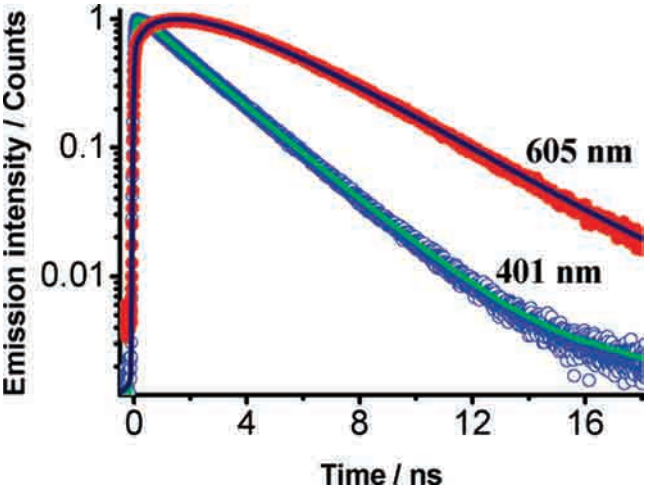

Figure 7. Time-resolved kinetics of N* (○) and C* (●) in water (pH 2) gated at 410 and 605 nm, respectively. The experimental fluorescence data for both N* and C* are compared with the numerical solution (solid lines) of the DSE model [green line, CPT(t); blue line, $CPTH^+(t)\exp(\tau/\tau_C)$], using the parameters of Table 6 and after convolution with the IRF. The blue line was corrected for the lifetime of the cation.

3.3. Application of the Debye−Smoluchowski Model. The emission decay curves in the equilibrium range were fit to the numerical solutions of the time-dependent Debye−Smoluchowski equation (DSE), which provides an adequate description for the proton diffusion from a photoexcited acid.[33,34] We resolved the problem using a user-friendly Windows application for spherically symmetric diffusion problems (SSDP, version 2.61).[35] The two-step scheme that we used is given in Scheme 5.

The first step, in which C* acts as an acid, involves protolytic dissociation to form the solvent ion pair $N^*\cdots H_3O^+$ with the intrinsic back proton-transfer rate constant k^*_{BPT}. The solvent ion pair can undergo an adiabatic recombination, described by the rate constant k^*_{DPT}. A diffusive second step follows the reversible reaction within the contact ion pair. Here, the hydrated proton is removed from the nearby associated molecule. The diffusion-controlled separation of the proton and N* is described by the DSE with the characteristic diffusion constant $D = D_{H^+} + D_{N^*}$ and the Debye radius R_D at pH 2. The fitting parameters are given in Table 6.

dx.doi.org/10.1021/jp201749u |J. Phys. Chem. A 2011, 115, 5094–5104

Figure 7 shows the experimental kinetics along with the fitting curves at pH 2. Both C* and N* kinetics were fit simultaneously using the same kinetic parameters, as listed in Table 6. The collision rate parameters were adjusted manually. The SSDP program was propagated on a spatial grid extending from 5.5 to 1500 Å, which, for the present parameters, is essentially infinity. We found good agreement between the ESPT rate constant values (k^*_{DPT}= 0.109 × 10^{10} s^{-1} and k^*_{BPT}= 8.60 × 10^7 s^{-1}, Table 6) and those obtained from the Birks model (k^*_{DPT} = 0.106 × 10^{10} s^{-1} and k^*_{BPT} = 8.33 × 10^7 s^{-1}, Table 5). The value of the excited-state equilibrium constant (pK^*_a= 1.78, Table 6) well matches that determined by the spectrofluorometric pH titration curves (pK^*_a = 1.85), thus demonstrating the reliability of using the above model to accurately describe proton diffusion at the related pH.

4. CONCLUSIONS

The results described and discussed in this work reveal the rich structural dynamics of CPT in acidic aqueous solutions. For solutions at pH < 2, the ESPT reaction of CPT is irreversible and leads to the formation of the red-emitting N-protonated quinolinium cation (τ_C = 2.83 ns). In the pH 1−2 range, a static quenching (K_S = 11.9 M^{-1}) of the fluorescence of N* by protons was found to accompany the overall dynamic quenching process (K_S = 70.6 M^{-1}). On the other hand, no protonation was observed at higher pH values (pH > 2), where N* is the only emitting species (τ_N = 3.76 ns). An excited-state equilibrium between the prototropic species is established only at pH 2 (pK^*_a = 1.85). The logarithmic dependence of the ESPT rate constant (k^*_{DPT}) on the proton activity ($a_{H_3O^+}$) clearly shows the existence of two structural regimes of proton motion. In the more acidic one (pH 0.9−1), the protonation of N* is independent of the diffusion, because of the existence of a ground-state complex between N and the proton. At pH > 1, the overall recombination process becomes a diffusion-controlled event, with ESPT rate constants that largely depend on the proton concentration (from 24 ps to almost 1 ns at pH 0.9 and 2, respectively). The number of protons involved in the proton transfer changes from ∼1 for the diffusive regime to ∼4 for the static one. A good fit to the experimental results in the equilibrium range (pH 2) was obtained using both the Birks and Smoluchowski models.

We believe that these results provide important information on the influence of the proton concentration on the photobehavior of the neutral and cationic structures of the drug, thus contributing to the overall understanding of the relationship between its structure and pharmacological activity.

■ ASSOCIATED CONTENT

Supporting Information. Absorption and emission spectra, and fluorescence decay of CPT in THF, absorption spectra in water at pH 0.9 and 4.4, curves for the determination of pK_a (S_0) and pK_a (S_1), normalized emission spectra in water at pH 1 and 2, details on the application of the Nernst equation, and Birks model to determine the rate constants involved in the proton-transfer and diffusion processes. This information is available free of charge via the Internet at http://pubs.acs.org.

■ AUTHOR INFORMATION

Corresponding Author

*E-mail: Abderrazzak.Douhal@uclm.es. Fax: +34-925-268840. Phone: +34-925-265717.

■ ACKNOWLEDGMENT

This work was supported by the MICINN through Project MAT2008-01609. M.R.d.N. thanks CYCLON Network (MRTN-CT-2008-Project 237962) for the Marie Curie fellowship. B.C. thanks MICINN for the Ramon y Cajal fellowship.

■ REFERENCES

(1) Wall, M. E.; Wani, M. C.; Cook, C. E.; Palmer, K. H.; McPhail, A. T.; Sims, G. A. *J. Am. Chem. Soc.* **1966**, *88*, 3888–3890.

(2) Gallo, R. C.; Whang-Peng, J.; Adamson, R. H. *J. Natl. Cancer Inst.* **1971**, *46*, 789–795.

(3) (a) Hsiang, Y.-H.; Hertzberg, R.; Hecht, S.; Liu, L. F. *J. Biol. Chem.* **1985**, *260*, 14873–14878. (b) Hsiang, Y.-H.; Liu, L. F. *Cancer Res.* **1988**, *48*, 1722–1726.

(4) Wall, M. E.; Wani, M. C.; Natschke, S. M.; Nicholas, A. W. *J. Med. Chem.* **1986**, *29*, 1553–1555.

(5) (a) Siu, F. M.; Che, C. M. *J. Am. Chem. Soc.* **2008**, *130*, 17928–17937. (b) Jena, N. R.; Mishra, P. C. *J. Mol. Model.* **2007**, *13*, 267–274.

(6) (a) Das, K.; Smirnov, A. V.; Wen, J.; Miskovsky, P.; Petrich, J. W. *Photochem. Photobiol.* **1999**, *69*, 633. (b) Solntsev, K. M.; Sullivan, E. N.; Tolbert, L. M.; Ashkenazi, S.; Leiderman, P.; Huppert, D. *J. Am. Chem. Soc.* **2004**, *126*, 12701. (c) El-Kemary, M.; Gil, M.; Douhal, A. *J. Med. Chem.* **2007**, *50*, 2896. (d) Gil, M.; Douhal, A. *J. Phys. Chem. A* **2008**, *112*, 8231. (e) Cohen, B.; Organero, J. A.; Santos, L.; Padial, L. R.; Douhal, A. *J. Phys. Chem. B* **2010**, *114*, 14787.

(7) For selected reviews, see: (a) Rivory, L. P.; Robert, J. *Pharmacol. Ther.* **1995**, *68*, 269–296. (b) Du, W. *Tetrahedron* **2003**, *59*, 8649–8687.

(8) For selected recent examples, see: (a) Servais, A.; Azzouz, M.; Lopes, D.; Courillon, C.; Malacria, M. *Angew. Chem., Int. Ed.* **2007**, *46*, 576–579. (b) Chavan, S. P.; Pathak, A. B.; Kalkote, U. R. *Synlett* **2007**, 2635–2638. (c) Liu, G.-S.; Dong, Q.-L.; Yao, Y.-S.; Yao, Z.-J. *Org. Lett.* **2008**, *10*, 5393–5396. (d) Pin, F.; Comesse, S.; Sanselme, M.; Daich, A. *J. Org. Chem.* **2008**, *73*, 1975–1978. (e) Ju, Y.; Liu, F.; Li, C. *Org. Lett.* **2009**, *11*, 3582–3585. (f) Mathijssen, R. H. J.; van Alphen, R. J.; Verweij, J.; Loos, W. J.; Nooter, K.; Stoter, G.; Sparreboom, A. *Clin. Cancer Res.* **2001**, *7*, 2182–2194. (g) Wallace, B. D.; Wang, H.; Lane, K. T.; Scott, J. E.; Orans, J.; Koo, J. S.; Venkatesh, M.; Jobin, C.; Yeh, L.-A.; Mani, S.; Redinbo, M. R. *Science* **2010**, *330*, 831–835.

(9) Fassberg, J.; Stella, V. J. *J. Pharm. Sci.* **1992**, *81*, 676–684.

(10) (a) Dey, J. I.; Warner, M. *J. Photochem. Photobiol. A* **1996**, *101*, 21–27. (b) Dey, J.; Warner, I. M. *J. Lumin.* **1997**, *71*, 105–114. (c) Dey, J.; Warner, I. M. *J. Photochem. Photobiol. A* **1998**, *116*, 27–37. (d) Biswas, A.; Dey, J. *Indian J. Chem. A* **2001**, *40*, 1143–1148.

(11) (a) Fleury, F.; Kudelina, I.; Nabiev, I. *FEBS Lett.* **1997**, *406*, 151–156. (b) Nabiev, I.; Fleury, F.; Kudelina, I.; Pommier, Y.; Charton, F.; Riou, J.-F.; Alix, A. J. P.; Manfait, M. *Biochem. Pharmacol.* **1998**, *55*, 1163–1174. (c) Chourpa, I.; Millot, J.-M.; Sockalingum, G. D.; Riou, J.-F.; Manfait, M. *Biochim. Biophys. Acta* **1998**, *1379*, 353–366. (d) Chourpa, I.; Riou, J.-F.; Millot, J.-M.; Pommier, Y.; Manfait, M. *Biochemistry* **1998**, *37*, 7284–7291. (e) Chauvier, D.; Chourpa, I.; Maizieres, M.; Riou, J.-F.; Dauchez, M.; Alix, A. J. P.; Manfait, M. *J. Mol. Struct.* **2003**, *651*, 55–65.

(12) (a) Burke, T. G.; Mi, Z. *J. Med. Chem.* **1994**, *37*, 40–46. (b) Mi, Z.; Burke, T. G. *Biochemistry* **1994**, *33*, 10325–10336. (c) Mi, Z.; Burke, T. G. *Biochemistry* **1994**, *33*, 12540–12545. (d) Burke, T. G.; Malak, H.; Gryczynski, I.; Mi, Z.; Lakowicz, J. R. *Anal. Biochem.* **1996**, *242*, 266–270.

(13) Posokhov, Y.; Biner, H.; Icüli, S. *J. Photochem. Photobiol. A* **2003**, *158*, 13–20.

(14) Jackson, G.; Porter, G. *Proc. R. Soc. London, Ser. A* **1961**, *260*, 13–30.

(15) (a) Weller, A. *Prog. React. Kinet.* **1961**, *1*, 189–214. (b) Malkin, Y. N; Kuz'min, V. A. *Russ. Chem. Rev.* **1990**, *59*, 164–178.

(16) Albert, A.; Phillips, J. N. *J. Chem. Soc.* **1956**, 1294–1304.

(17) Solntsev, K. M.; Sullivan, E. N.; Tolbert, L. M.; Ashkenazi, S.; Leiderman, P.; Huppert, D. *J. Am. Chem. Soc.* **2004**, *126*, 12701−12708 and references therein.

(18) Burke, T. G.; Mishra, A. K.; Wani, M. C.; Wall, M. E. *Biochemistry* **1993**, *32*, 5352–5364.
(19) Pines, E.; Magnes, B.-Z.; Lang, M. J.; Fleming, G. R. *Chem. Phys. Lett.* **1997**, *281*, 413–420.
(20) Rini, M.; Magnes, B.-Z.; Pines, E.; Nibbering, E. T. J. *Science* **2003**, *301*, 349–352.
(21) Janz, G. J.; Tomkins, R. P. T. *Nonaqueous Electrolytes Handbook*; Plenum Press: New York, 1973.
(22) Erdey-Grúz, T. *Transport Phenomena in Aqueous Solutions*; Adam Hilger Ltd.: London, 1974.
(23) Data from: Conway, B. B. *Electrochemical Data*; Elsevier: New York, 1952.
(24) (a) Cukierman, S. *Biophys. J.* **2000**, *78*, 1825−1834 and references therein. (b) Marx, D.; Tuckerman, M. E.; Hutter, J. Parrinello, M. *Nature* **1999**, *397*, 601−604 and references therein. (c) Laage, D.; Hynes, J. T. *Science* **2006**, *311*, 832–835. (d) Laage, D.; Hynes, J. T. *J. Phys. Chem. B* **2008**, *112*, 14230–14242. (e) Headrick, J. M.; Diken, E. G.; Walters, R. S.; Hammer, N. I.; Christie, R. A.; Cui, J.; Myshakin, E. M.; Duncan, M. A.; Johnson, M. A.; Jordan, K. D. *Science* **2005**, *308*, 1765–1769. (f) Timmer, R. L. A.; Tielrooij, K. J.; Bakker, H. J. *J. Chem. Phys.* **2010**, *132*, 194504–194504−9.
(25) Bresiau, B. R.; Miller, I. F. *J. Phys. Chem.* **1970**, *74*, 1056–1061.
(26) Eigen, M. *Angew. Chem., Int. Ed. Engl.* **1964**, *3*, 1–19.
(27) Birks, J. B. *Photophysics of Aromatic Molecules*; Wiley: London, 1970.
(28) (a) Ghosh, S. K. *J. Mol. Liq.* **1993**, *57*, 75−90 and references therein. (b) Douhal, A.; Lahmani, F.; Zewail, A. H. *Chem. Phys.* **1996**, *207*, 477–498.
(29) Bardez, E.; Fedorov, A.; Berberan-Santos, M. N.; Martinho, J. M. G. *J. Phys. Chem. A* **1999**, *103*, 4131−4136 and references therein.
(30) MacInnes, D. A. *J. Am. Chem. Soc.* **1919**, *41*, 1086–1092.
(31) Kim, T. G.; Kim, Y.; Jang, D.-J. *J. Phys. Chem. A* **2001**, *105*, 4328–4332.
(32) Fecko, C. J.; Eaves, J. D.; Loparo, J. J.; Tokmakoff, A.; Geissler, P. L. *Science* **2003**, *301*, 1698–1702.
(33) Solntsev, K. M.; Huppert, D.; Agmon, N.; Tolbert, L. M. *J. Phys. Chem. A* **2000**, *104*, 4658–4669.
(34) (a) Gopich, I. V.; Solntsev, K. M.; Agmon, N. *J. Chem. Phys.* **1999**, *110*, 2164–2174. (b) Agmon, N. *J. Chem. Phys.* **1999**, *110*, 2175–2180. (c) Solntsev, K. M.; Agmon, N. *Chem. Phys. Lett.* **2000**, *320*, 262–268.
(35) Krissinel', E. B.; Agmon, N. *J. Comput. Chem.* **1996**, *17*, 1085–1098.